AVAILABILITY OF GAST D GBAS CONSIDERING CONTINUITY OF AIRBORNE MONITORS[*]

Curtis A. Shively
Thomas T. Hsiao
Center for Advanced Aviation System Development
The MITRE Corporation, McLean VA

BIOGRAPHIES

Curtis A. Shively is a member of the Principal Staff at MITRE/CAASD. He has studied the use of satellites for communications, navigation and surveillance. He received his B.S. and M.S. in Electrical Engineering from the Massachusetts Institute of Technology.

Thomas T. Hsiao is a Lead Staff at MITRE/CAASD. He has made significant contributions to availability analyses of GPS for navigation systems including both LAAS and WAAS. He received his M.S. degree in Electrical Engineering from University of Akron, Ohio.

ABSTRACT

Standards are being developed for using a ground based augmentation system (GBAS) to provide guidance for CAT III approach and landing operations, known as GBAS Approach Service Type D (GAST D). To evolve from CAT I (GAST C) to GAST D an additional method for mitigating potential errors due to ionospheric anomalies must be implemented in the aircraft. This paper considers the continuity risk from monitors and protection levels affected by this additional ionospheric anomaly mitigation. Three such processes are analyzed: 1) dual smoothing ionospheric gradient monitoring algorithm (DSIGMA) monitor, 2) fault-free vertical protection level (VPL_{H0}) and 3) reference receiver fault monitor (RRFM). A geometry constraint needed to independently ensure acceptable continuity risk for each process is first identified. The constraint needed for RRFM has already been included in specifications. However, only geometry constraints needed for adequate integrity protection with DSIGMA have been specified. Thus, the analysis assesses whether continuity constraints for DSIGMA and VPL_{H0} must also be implemented. The analysis determines the continuity risk from enforcing all or only some of these constraints. Results show that the VPL_{H0} continuity risk predominates and a corresponding constraint is needed. However, given only the constraint for VPL_{H0} the continuity risk from DSIGMA could arguably be acceptable. Moreover, even if all constraints are enforced availability of adequate satellite geometry is no less than that limited by the separate geometry constraints needed for proper integrity protection with DSIGMA.

INTRODUCTION

Background

Concepts have been developed and standards are being finalized for using a ground based augmentation system (GBAS) to provide guidance for CAT III approach and landing operations, known as GBAS Approach Service Type D (GAST D) [1, 2, 3]. The evolution of CAT I GBAS (GAST C) to GAST D has involved some changes and additions to monitors and protection levels in the airborne equipment. In particular, in order to mitigate the effect of ionospheric anomalies, the GAST D airborne equipment will compute the difference between vertical position solutions based on data and corrections smoothed with 30 s time constant and those smoothed with 100 s time constant. Comparison of the magnitude of this difference, D_V, to a threshold will be done by a dual smoothing ionospheric gradient monitoring algorithm (DSIGMA) [4]. Some aircraft-dependent geometry constraints will also be enforced to limit the error due to ionospheric anomalies not detected by DSIGMA [3, 4]. To further mitigate the effects of ionospheric anomalies, aircraft guidance will be based on the 30 s solution. However, integrity data broadcast from the ground are associated primarily with the 100 s solution. Therefore, protection levels and other fault monitors operating in the aircraft must also include the D_V term (and an analogous

---

[*] The contents of this material reflect the views of the authors. Neither the Federal Aviation Administration nor the Department of Transportation makes any warranty or guarantee, or promise, expressed or implied concerning the content or accuracy of the views expressed herein.
©2009 The MITRE Corporation

D_L term if applied in the lateral dimension) to ensure integrity of the 30 s solution used for guidance.

Purpose and Organization of Paper

This paper considers the continuity risk from monitors and protection levels due to effects of the new GAST D ionospheric mitigation in the aircraft. The paper begins with discussion of a model for the characteristics of the vertical difference, $V_{diff,}$ between the 30 s solution and the 100 s solution. Then the paper presents a brief summary of each monitor and protection level that includes D_V, the magnitude of V_{diff}. Separate subsections are included for the DSIGMA monitor, the fault-free vertical protection level (VPL_{H0}) and the reference receiver fault monitor (RRFM). Each section identifies the geometry constraint needed to independently ensure a continuity risk allocation for each monitor or protection level. The actual continuity risk allocations that have been previously proposed for GAST D are then summarized. Then theoretical predictions for the effect of each constraint on limiting the standard deviation of V_{diff} are derived. Continuity results are presented and compared to the theoretical predictions to indicate the interplay of the various constraints. Finally availability results are presented for various cases of implementing some or all of the constraints. The paper concludes with a summary.

CHARACTERIZATION OF VERTICAL SOLUTION DIFFERENCE V_{diff}

Let the vertical component of the difference between position solutions based on 30 s smoothing and 100 s smoothing be denoted V_{diff}. Then D_V is the magnitude of that difference

$$D_V = \left| V_{diff} \right| \tag{1}$$

Although V_{diff} is defined in terms of a difference in the position domain, it can also be expressed in terms of differences of the underlying range domain quantities for individual satellites as follows

$$V_{diff} = \sum_{i=1}^{N} S_{vert,i} \times D_{R,i} \tag{2}$$

Where for the ith satellite, $D_{R,i}$ is the difference between the differentially corrected range based on 30 s smoothed data and the differentially corrected range based on 100 s smoothed data. It should be pointed out that identical vertical coefficients, $S_{vert,i}$ based on geometry and the error model weighting matrix for the 100 s data, are used to calculate both the 30 s solution and the 100 s solution [3].

In order to determine the statistical characteristics of V_{diff} it is necessary to have a model for $D_{R,i}$. A simplified model has been suggested by Mats Brenner of Honeywell and Tim Murphy of Boeing [5]. This model is based on the assumption that $D_{R,i}$ primarily reflects only the difference in the corrected range errors due to ionospheric delay. For a particular smoothing time constant (first order filter), τ, the residual error due to ionospheric delay after application of differential corrections is given by [6]

$$\begin{aligned} E_{iono}(\tau) &= Obliquity(\theta_i) \\ &\times G_{vert\_iono\_gradient} \\ &\times \left(X_{\text{dist\_to\_gf}} + 2 \times \tau \times V_{air} \right) \end{aligned} \tag{3}$$

Where the Obliquity factor is related to the satellite elevation angle θ_i by [6]

$$Obliquity(\theta_i) = \frac{1}{\sqrt{1 - (0.948 \times \cos(\theta_i))^2}} \tag{4}$$

$G_{vert\_iono\_gradient}$ is the spatial gradient of the ionospheric vertical delay, $X_{dist\_to\_gf}$ is the distance of the aircraft from the ground facility and V_{air} is the aircraft velocity. It is useful to point out that $E_{iono}(\tau)$ consists of contributions from two effects. The first is caused by the difference in ionospheric delay at the aircraft and the ground facility just due to the separation between them. This effect does not depend on the smoothing filter time constant. The second effect is caused by the lag in the smoothing filter responding to change in delay over time as the aircraft moves through the ionospheric delay spatial gradient. This lag depends on the smoothing filter time constant. $D_{R,i}$ is just the difference between the values of $E_{iono}(\tau)$ for $\tau = 30$ and $\tau = 100$

$$\begin{aligned} D_{R,i} &= E_{iono}(30) - E_{iono}(100) \\ &= -Obliquity(\theta_i) \\ &\times G_{vert\_iono\_gradient} \times 140 \times V_{air} \end{aligned} \tag{5}$$

Note that the effect caused by separation of the aircraft from the ground station cancels and the result is just the difference in the effect due to the lag of each smoothing filter.

The ionospheric gradient is assumed to be normally distributed with zero mean and standard deviation denoted $\sigma_{vert\_iono\_gradient}$. Therefore, the standard deviation of D_R is given as a function of elevation angle θ by

2

$$\sigma_{D_R}(\theta) = Obliquity(\theta)$$
$$\times \sigma_{vert\_iono\_gradient} \times 140 \times V_{air}$$

(6)

For the analysis it will be further assumed that $\sigma_{vert\_iono\_gradient}$ = 4 mm/km [7] and that V_{air} = 140 kts = 0.072 km/s. Substituting these values into equation (6) gives

$$\sigma_{D_R}(\theta) = Obliquity(\theta) \times 0.004 \times 140 \times 0.072$$
$$= Obliquity(\theta) \times 0.04 \text{ m}$$

(7)

A graph of σ_{DR} versus θ is shown in Figure 1. Note that at low elevation angles, the value of σ_{DR} increases to approximately 3×0.04 m = 0.12 m. The graph also shows a plot of σ_{100}, the standard deviation of the differentially corrected range error for 100 s smoothing. In addition to the ionospheric error for 100 s smoothing, the values of σ_{100} include ground station error for ground accuracy designator C with 4 reference stations (GADC-4) [8], and airborne error for accuracy designator B (AAD-B) [8] and multipath designator A (AMD-A) [8]. The graph assumes that the error due to tropospheric delay is negligible (after differential correction). Note the model gives values for σ_{DR} that are much smaller than those for σ_{100}. This is as it should be, since the errors in the 100 s smoothed data and the 30 s smoothed data are likely to be highly correlated and their difference should be very small in comparison to either one.
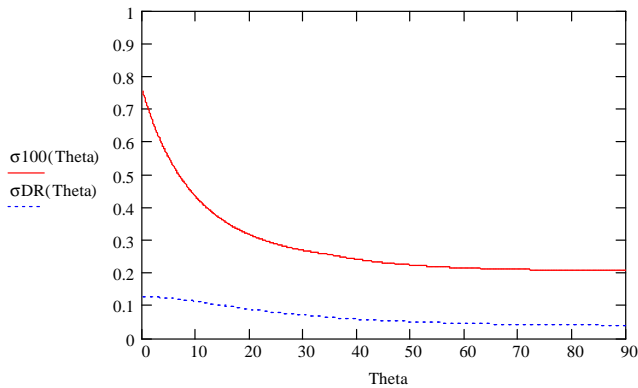

Figure 1. Graph of σ_{DR} and σ_{100} versus Elevation Angle

For use later in the analysis it is convenient to determine the ratio of σ_{DR} to σ_{100}

$$R_R(\theta) = \frac{\sigma_{DR}(\theta)}{\sigma_{100}(\theta)}$$

(8)

A plot of this ratio versus θ is given in Figure 2. Note that the maximum value of R_R is 0.281 and the minimum value is 0.167.
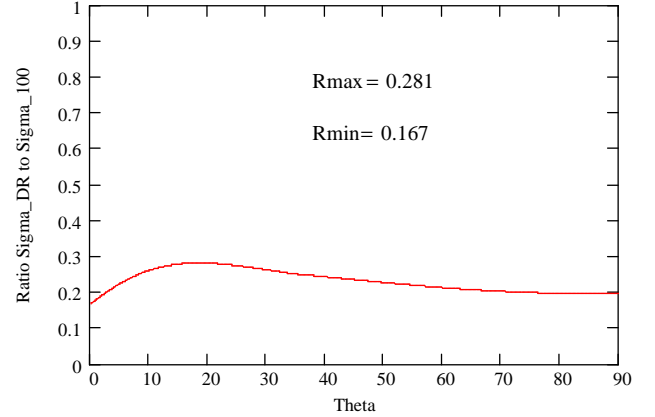

Figure 2. Graph of Ratio of σ_{DR} to σ_{100} versus Elevation Angle

Based on the assumption that the gradient is Normally distributed and equation (2), it is evident that V_{diff} is a Normally distributed random variable with standard deviation σ_{Vdiff} given by

$$\sigma_{V_{diff}} = \sqrt{\sum_{i=1}^{N} S_{vert,i}^2 \times \sigma_{D_R}^2(\theta_i)}$$

(9)

MONITORS AND PROTECTION LEVELS USING D_V

DSIGMA Monitor

The DSIGMA monitor applies a fixed threshold of 2 m to D_V [3], i.e, to the magnitude of V_{diff}

$$\left| V_{diff} \right| \leq 2 \text{ m}$$

(10)

Therefore, the continuity risk from the DSIGMA monitor varies with the actual geometry and is given by

$$CR_{DSIGMA} = 2 \times Q(K_{DSIGMA})$$

(11)

Where Q(K) is computed from

$$Q(K) = \int_{K}^{\infty} \frac{1}{\sqrt{2\pi}} e^{-\frac{x^2}{2}} dx$$

(12)

3

And K_{DSIGMA} is the equivalent threshold K factor of the DSIGMA monitor

$$K_{DSIGMA} = \frac{2}{\sigma_{V_{diff}}} \qquad (13)$$

It should be mentioned at this point in the discussion that the threshold of 2 m for DSIGMA provides adequate integrity protection for ionospheric anomaly errors only if limits are placed on the S_{vert} coefficients [3]. Such limits would in practice be aircraft specific related to the landing performance and largest undetected error that is deemed tolerable. Representative limits [9] are

$$\left| S_{vert,i} \right| \le 4.0 \qquad (14)$$

for any single satellite and

$$\left| S_{vert,i} \right| + \left| S_{vert,j} \right| \le 6.0 \qquad (15)$$

for any pair of satellites.

VPL$_{H0}$

The VPL$_{H0}$ protection level represents a bound on the vertical position error in the fault-free condition (H$_0$ hypothesis). For GAST C (CAT I) VPL$_{H0}$ is computed as a factor K_{ffmd} times the vertical standard deviation of the position solution in the fault-free condition, $\sigma_{vert,100}$

$$VPL_{H0} = K_{ffmd} \times \sigma_{vert,100} \text{ for GAST C} \quad (16)$$

Where

$$\sigma_{vert,100} = \sqrt{\sum_{i=1}^{N} S_{vert,i}^2 \times \sigma_{100}^2(\theta_i)} \qquad (17)$$

For CAT III (GAST D), since guidance is based on the 30 s solution, D_V must be added to the CAT I protection level [3]

$$\begin{aligned} VPL_{H0} = K_{ffmd} \times \sigma_{vert,100} + D_V \\ \text{for GAST D} \end{aligned} \qquad (18)$$

For any acceptable satellite geometry the value of VPL$_{H0}$ must not exceed the vertical alert limit (VAL) [3]

$$VPL_{H0} \le VAL \qquad (19)$$

Thus, from equations (18) and (19) it is evident that there is an effective threshold on the real time values of D$_V$, i.e., on the magnitude of V$_{diff}$

$$D_V \le VAL - K_{ffmd} \times \sigma_{vert,100} \qquad (20)$$

Therefore, the continuity risk from VPL$_{H0}$ varies with the actual satellite geometry and is given by

$$CR_{VPLH0} = 2 \times Q(K_{VPLH0}) \qquad (21)$$

where K_{VPLH0} is the equivalent threshold K factor of VPL$_{H0}$

$$K_{VPLH0} = \frac{VAL - K_{ffmd} \times \sigma_{vert,100}}{\sigma_{V_{diff}}} \qquad (22)$$

Where σ_{Vdiff} is defined in equation (9).

RRFM

For GAST D the threat of single ground reference receiver (RR) faults (H$_1$ hypothesis) is mitigated by an error estimation process in the ground station and a monitor in the aircraft [3, 10]. The ground facility computes B-values which estimate the error in the broadcast correction caused by a fault of a single reference receiver. The B-value for measurements of the ith satellite on the jth RR is computed by comparing the correction from the jth RR to the average of the corrections for the same satellite from the other RRs

$$B_{i,j} = \frac{1}{M[i]} \left(C_{i,j} - \frac{\sum_{\substack{k=1 \\ k \ne j}}^{M[i]} C_{i,k}}{M[i]-1} \right) \qquad (23)$$

Where M[i] is the number of RRs (typically 4) whose corrections are included in the broadcast average correction for the ith satellite and C$_{i,k}$ is the correction for the ith satellite from the kth RR. Of course the comparison is scaled by the factor 1 / M[i] to reflect the effect of a fault on the jth RR in the average correction for the ith satellite.

The B-values are broadcast to the aircraft where they are combined with the position solution vertical geometry coefficients (S$_{vert,i}$) to form an estimate of the vertical error. Since the B-values are based on 100 s corrections,

4

but the aircraft uses the 30 s solution for guidance, the error estimate also includes D_V. The resulting vertical error estimate under the hypothesis of a faulty j^{th} RR is then

$$Vest_{H1,j} = \left| \sum_{i=1}^{N} S_{vert,i} \times B_{i,j} \right| + D_V \qquad (24)$$

The reference receiver fault monitor (RRFM) in the aircraft applies a threshold to this vertical error estimate

$$Vest_{H1,j} \leq T_{BAC} \qquad (25)$$

The threshold T_{BAC} is chosen as

$$T_{BAC} = K_{RRFM} \times \sigma_{DS} \qquad (26)$$

Where

$$\sigma_{DS} = \sqrt{\sigma_{B,vert}^2 + \sigma_{V_{diff}}^2} \qquad (27)$$

And where

$$\sigma_{B,vert} = \sqrt{\sum_{i=1}^{N} S_{vert,i}^2 \frac{\sigma_{pr\_gnd,i}^2(\theta_i)}{M[i]-1}} \qquad (28)$$

Where σ_{pr_gnd} is the contribution from the ground station to the error in the differential correction. The value of K_{RRFM} is chosen as small as possible consistent with acceptable continuity risk. The value assumed for the analysis is 5.5, the minimum allowed by [3].

It might at first be thought that the continuity risk for the RRFM would be computed as $2 \times Q(K_{RRFM}) = 2 \times Q(5.5) = 4 \times 10^{-8}$. However, close inspection of equation (24) reveals that in the fault-free case $Vest_{H1,j}$ is the sum of the magnitudes of two Gaussian random variables whose standard deviations are root-sum-squared in equation (27) to obtain σ_{DS}. Thus, the probability that the sum of the magnitudes exceeds a given value now includes the combinations where the two random variables have opposite sign in addition to the two cases where they have the same sign. Consequently, the continuity risk is essentially doubled and is found by direct integration of the magnitude density functions to be approximately 8×10^{-8}.

Note that setting the threshold T_{BAC} as in equation (26) with K_{RRFM} always equal to 5.5 gives a continuity risk always equal to 8×10^{-8} regardless of satellite geometry.

However, T_{BAC} cannot be allowed to increase indefinitely as the satellite geometry gets worse. Obviously, as T_{BAC} increases, the minimum size error that the monitor will miss with an acceptable probability increases. Therefore, there must be a limit on T_{BAC} based on meeting requirements for safety of the CAT III landing. The largest acceptable value of T_{BAC} depends on the landing characteristics of a particular aircraft. Therefore, a detailed discussion of determining a limit on T_{BAC} is beyond the scope of this current paper. However, in [10] it was shown that a maximum T_{BAC} of approximately 3.8 m would allow safety of landing requirements to be met for representative aircraft landing characteristics. Therefore, it will be assumed in the analysis that

$$T_{BAC} \leq 3.8\,\text{m} \qquad (29)$$

Combining equation (29) with equation (26) and using the assumed value of $K_{RRFM} = 5.5$ gives the following constraint on σ_{DS}

$$\sigma_{DS} = \frac{T_{BAC}}{K_{RRFM}} \leq \frac{3.8}{5.5} = 0.691\,\text{m} \qquad (30)$$

CONTINUITY RISK ALLOCATIONS

The overall continuity risk allocation for GAST D is still under discussion as of this writing. However, a total allocation of 10^{-5} per operation has been proposed [1]. The operation includes a period of 15 s when both the lateral and vertical guidance must be maintained during the critical time just prior to crossing the runway threshold followed by another period of 15 s when only the lateral guidance is of concern during the flare, touchdown and roll-out [1]. Of interest in this paper are the continuity risk allocations to processes in the aircraft during the 15 s when the vertical guidance is of concern. An example in [1] proposes that 1.5×10^{-7} be allocated to airborne monitors and that 4×10^{-8} be allocated to protection levels exceeding alert limits with no configuration change (no loss of satellite or ground reference receiver). It should be noted that the above allocations apply to the total of both vertical and lateral continuity risk. However, for this analysis the entire allocation for each case will be associated with only the vertical continuity risk since the application of monitors and protection level limits is always more constraining in the vertical dimension. It is further reiterated in [1] that these allocations must apply to any specific satellite subset geometry that could be used for navigation.

5

THEORETICAL RESTRICTIONS ON σ_{Vdiff} DUE TO EACH CONTINUITY CONSTRAINT

It is useful at this point in the discussion to derive the largest value of σ_{Vdiff} that would theoretically be allowed by each separate continuity constraint for RRFM, DSIGMA or VPL_{H0} or by VPL_{H0} without any allowance for continuity risk. The constraints for continuity risk will be derived assuming the above allocations are met. These predictions are useful for investigating which constraints may predominate over others and therefore whether all constraints must actually be implemented to limit the continuity risk as desired.

Limit on σ_{Vdiff} Due to DSIGMA Continuity Constraint

Since the total continuity allocation for monitors is 1.5×10^{-7} and the RRFM monitor is designed to always achieve 8×10^{-8}, a residual sub-allocation of 7×10^{-8} will be assumed for DSIGMA. The corresponding minimum value of K_{DSIGMA} is 5.4. The corresponding limit on σ_{Vdiff} is found using equation (13) to be

$$\sigma_{V_{diff}} \leq \frac{2}{5.4} = 0.37 \text{ m} \tag{31}$$

Limit on σ_{Vdiff} from VPL_{H0} With Continuity Constraint

The sub-allocation of 4×10^{-8} for protection levels exceeding alert limits with no configuration change will be assumed to be completely allocated to VPL_{H0}. The corresponding minimum value of K_{VPLH0} is 5.5. From equation (22)

$$K_{VPLH0}$$
$$= \frac{VAL - K_{ffmd} \times \sigma_{vert,100}}{\sigma_{V_{diff}}} \geq 5.5 \tag{32}$$

A constraint on σ_{Vdiff} can be found by assuming a relationship between σ_{Vdiff} and $\sigma_{vert,100}$. Suppose for the moment that

$$\sigma_{V_{diff}} = R_V \times \sigma_{vert,100} \tag{33}$$

Then substituting from equation (33) into equation (32) gives

$$\frac{VAL - K_{ffmd} \times \dfrac{\sigma_{V_{diff}}}{R_V}}{\sigma_{V_{diff}}} \geq 5.5 \tag{34}$$

Solving equation (34) for σ_{Vdiff} establishes the following upper limit

$$\sigma_{V_{diff}} \leq \frac{VAL}{5.5 + \dfrac{K_{ffmd}}{R_V}} \tag{35}$$

To establish the value of R_V recall the above discussion regarding $R_R(\theta)$, the ratio of $\sigma_{DR}(\theta)$ to $\sigma_{100}(\theta)$ (equation (8)). Using $R_R(\theta)$ in the expression for σ_{Vdiff} from equation (9) gives

$$\sigma_{V_{diff}} = \sqrt{\sum_{i=1}^{N} S_{vert,i}^2 \times \sigma_{D_R}^2(\theta_i)}$$
$$= \sqrt{\sum_{i=1}^{N} S_{vert,i}^2 \times R_R^2(\theta_i) \times \sigma_{100}^2(\theta_i)} \tag{36}$$

Then if

$$R_{min} \leq R_R(\theta_i) \leq R_{max} \tag{37}$$

It follows that

$$R_{min} \times \sqrt{\sum_{i=1}^{N} S_{vert,i}^2 \times \sigma_{100}^2(\theta_i)}$$
$$\leq \sqrt{\sum_{i=1}^{N} S_{vert,i}^2 \times R_R^2(\theta_i) \times \sigma_{100}^2(\theta_i)} \tag{38}$$
$$\leq R_{max} \times \sqrt{\sum_{i=1}^{N} S_{vert,i}^2 \times \sigma_{100}^2(\theta_i)}$$

Substituting the expression for $\sigma_{vert,100}$ from equation (17) into equation (38) gives

$$R_{min} \times \sigma_{vert,100} \leq \sigma_{V_{diff}} \leq R_{max} \times \sigma_{vert,100} \tag{39}$$

Or alternatively

$$R_{min} \leq R_V \leq R_{max} \tag{40}$$

Substituting the values shown in Figure 2 of $R_{max} = 0.281$ and $R_{min} = 0.167$ for R_V in equation (35) and further assuming VAL = 10.0 m and $K_{ffmd} = 5.84$ gives a maximum value of σ_{Vdiff} ranging from 0.247 m to 0.380 m.

6

Limit on σ_{Vdiff} from VPL_{H0} Without Continuity Constraint

Even without including a continuity constraint for D_V, the requirement to have VPL_{H0} less than VAL gives a limit on $\sigma_{vert,100}$ and therefore indirectly a limit on σ_{Vdiff}. Ignoring D_V in equation (18) and making use of equation (19) gives

$$K_{ffmd} \times \sigma_{vert,100} \le VAL \tag{41}$$

And the following limit on $\sigma_{vert,100}$

$$\sigma_{vert,100} \le \frac{VAL}{K_{ffmd}} = \frac{10}{5.84} = 1.71\,\text{m} \tag{42}$$

Making use of equation (42) in equation (39) gives

$$R_{min} \times 1.71 \le \sigma_{V_{diff}} \le R_{max} \times 1.71 \tag{43}$$

And substituting the values of $R_{max} = 0.281$ and $R_{min} = 0.167$ gives a maximum value of σ_{Vdiff} ranging from 0.286 m to 0.481 m.

Limit on σ_{Vdiff} from RRFM

Recalling from the discussion of RRFM above and equation (30) the limit on σ_{DS} is

$$\sigma_{DS} \le 0.691\,\text{m} \tag{44}$$

Substituting for σ_{DS} using equation (27) gives

$$\sqrt{\sigma_{B,vert}^2 + \sigma_{V_{diff}}^2} \le 0.691\,\text{m} \tag{45}$$

A corresponding limit on σ_{Vdiff} can be obtained by establishing a relationship between σ_{Vdiff} and $\sigma_{B,vert}$. This may be accomplished by first finding the ratio R_B of $\sigma_{B,vert}$ to $\sigma_{vert,100}$

$$\sigma_{B,vert} = R_B \times \sigma_{vert,100} \tag{46}$$

And then making use of this relationship in equation (33) that relates σ_{Vdiff} to $\sigma_{vert,100}$.

$$\sigma_{B,vert} = R_B \times \sigma_{vert,100} = \frac{R_B}{R_V} \times \sigma_{V_{diff}} \tag{47}$$

Substituting equation (47) into equation (45) and solving for σ_{Vdiff} gives

$$\sigma_{V_{diff}} \le \frac{0.691\,\text{m}}{\sqrt{\left(\dfrac{R_B}{R_V}\right)^2 + 1}} \tag{48}$$

Let $R_G(\theta)$ be the ratio of $\sigma_{pr\_gnd}(\theta)$ to $\sigma_{100}(\theta)$

$$\sigma_{pr\_gnd}(\theta) = R_G(\theta) \times \sigma_{100}(\theta) \tag{49}$$

It can be determined from examination of the error models for $\sigma_{pr\_gnd}(\theta)$ and $\sigma_{100}(\theta)$ that

$$0.159 \le R_G(\theta) \le 0.469 \tag{50}$$

Then from the definition of $\sigma_{B,vert}$ from equation (28) and assuming M[i] -1 is always equal to 3 gives

$$\begin{aligned}
\sigma_{B,vert} &= \frac{1}{\sqrt{3}} \sqrt{\sum_{i=1}^{N} S_{vert,i}^2 \times \sigma_{pr\_gnd,i}^2(\theta_i)} \\
&= \frac{1}{\sqrt{3}} \sqrt{\sum_{i=1}^{N} S_{vert,i}^2 \times R_G(\theta_i)\sigma_{100,i}^2(\theta_i)}
\end{aligned} \tag{51}$$

Making use of the limits on $R_G(\theta)$ from equation (50) and the expression for $\sigma_{vert,100}$ from equation (17) it can easily be shown that

$$\begin{aligned}
\frac{0.159}{\sqrt{3}} \times \sigma_{vert,100} &\le \sigma_{B,vert} \\
&\le \frac{0.469}{\sqrt{3}} \times \sigma_{vert,100}
\end{aligned} \tag{52}$$

Or alternatively

$$0.092 \le R_B \le 0.271 \tag{53}$$

Substituting the extremes of 0.092 and 0.271 for R_B and 0.167 and 0.281 for R_V (equation (40)) into equation (48) gives a maximum value of σ_{Vdiff} ranging from 0.363 m to 0.657 m.

7

THEORETICAL RESTRICTIONS ON CONTINUITY RISK DUE TO EACH CONTINUITY CONSTRAINT

VPL_{H0}

Of course, if the VPL_{H0} continuity constraint is applied, the theoretical limit on CR_{VPLH0} is the design limit, which in this case is 4.0×10^{-8}. If however, this constraint is not applied, but other constraints for RRFM and DSIGMA are applied, σ_{Vdiff} will be limited. However, geometries could still be allowed where $K_{ffmd} \times \sigma_{vert,100}$ approaches VAL. Therefore, there is no guarantee that there will be any margin for non-zero variations of D_V in the comparison of VPL_{H0} to VAL. Consequently, without the explicit VPL_{H0} continuity constraint applied, the theoretical limit on CR_{VPLH0} is 1.0.

DSIGMA

Table 1 summarizes the theoretical limits on continuity risk from DSIGMA if each constraint is applied individually giving the resulting limits on σ_{Vdiff} just derived above.

Table 1. DSIGMA Continuity Risk for Each Constraint Applied Separately

| Function	DSIGMA	H_0 with Continuity	H_0 w/o Continuity	RRFM
Max σ_{Vdiff} (m)	0.370	0.247 to 0.380	0.286 to 0.481	0.363 to 0.657
Max CR_{DSIGMA}[1]	7×10^{-8}	6.7×10^{-16} to 1.5×10^{-7}	3.1×10^{-12} to 3.3×10^{-5}	3.7×10^{-8} to 2.3×10^{-3}

[1] Calculated by substituting the maximum σ_{Vdiff} value into equation (13) and using in equation (11).

CONTINUITY RISK RESULTS

Representative continuity results will now be presented for Seattle for an idealized constellation consisting of 24 satellites in the primary orbital slots [11]. The graphs show the continuity risk at 5 minute intervals over the 24 hour day. The value shown at each time sample is the worst for any subset of visible satellites that meets the indicated geometry criteria. Different cases will be examined for whether or not the constraints for DSIGMA or VPL_{H0} are enforced. In all cases at least the following constraints are enforced: 1) S_{vert} for DSIGMA from equations (14) and (15), 2) RRFM from equation (30) and 3) VPL_{H0} without continuity consideration from equation (41).
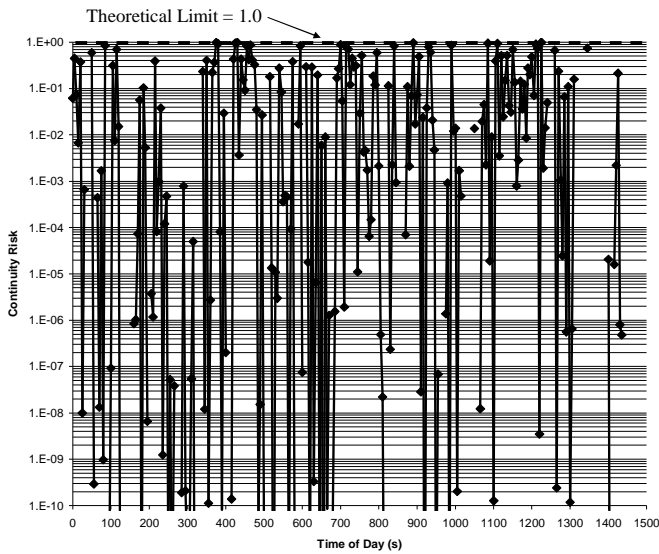
No Continuity Constraints for DSIGMA or VPL_{H0}

Continuity risk results with no continuity constraints for either DSIGMA or VPL_{H0} are shown in Figures 3 and 4. The result for DSIGMA continuity risk is given in Figure 3. Note that the largest worst-case risk values occasionally approach or just slightly exceed 10^{-5}. Referring back to Table 1 it can be seen that the theoretical maximum CR_{DSIGMA} as limited by RRFM is 2.3×10^{-3}. However, a lower theoretical maximum CR_{DSIGMA} of 3.3×10^{-5} is associated with the H0 w/o continuity limit. Note that the maximum values of about 1×10^{-5} in Figure 3 are just slightly less than the more restrictive prediction for VPL_{H0} w/o continuity. The results for VPL_{H0} continuity risk are given in Figure 4. Note that the worst-case risk values approach 1.0 as predicted.
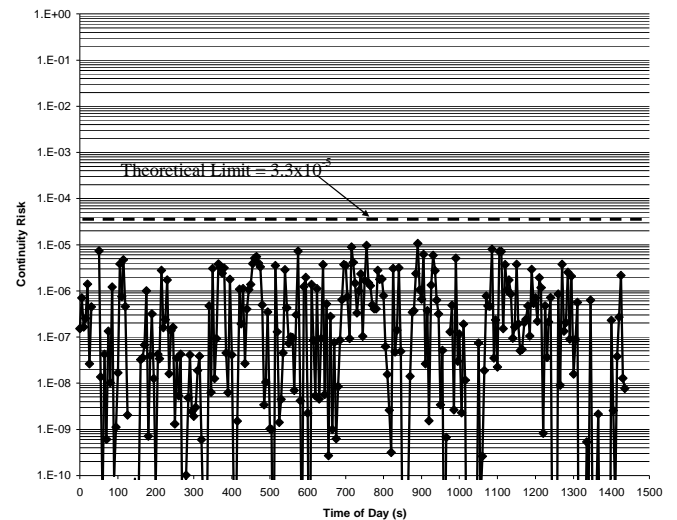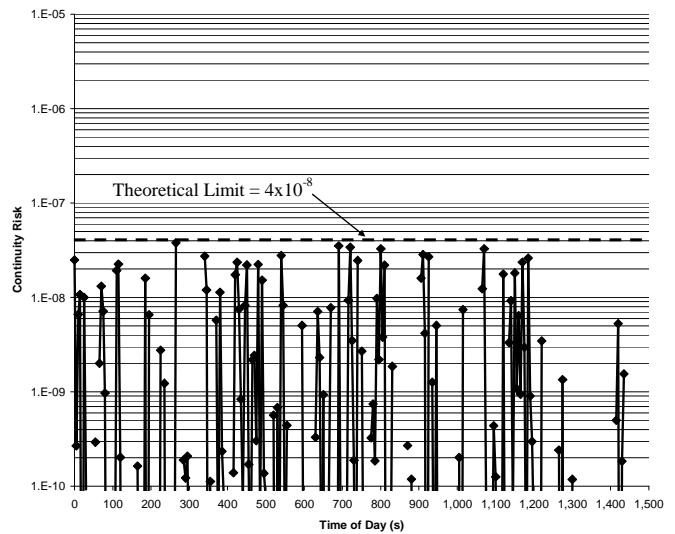

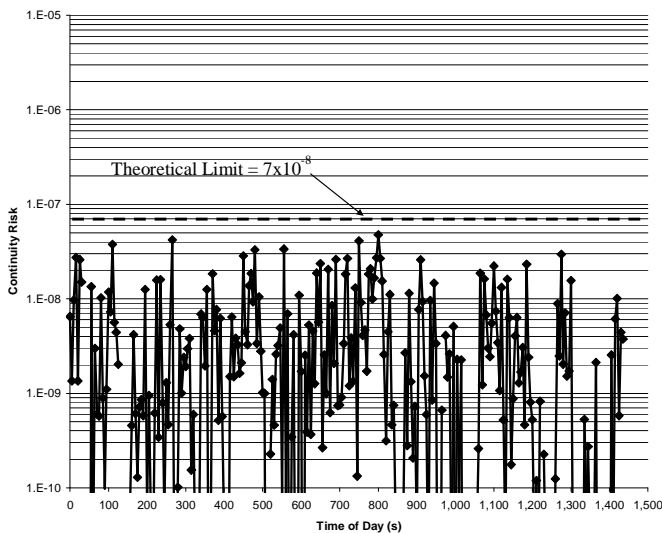**Figure 3. DSIGMA Continuity Risk with No Continuity Constraints for DSIGMA or VPL_{H0}**

Figure 4. VPL_{H0} Continuity Risk with No Continuity Constraints for DSIGMA or VPL_{H0}

Both DSIGMA and VPL_{H0} Constraints Applied

Continuity risk results with all constraints applied are shown in Figure 5 for DSIGMA and in Figure 6 for VPL_{H0}. Note that the largest values of CR_{DSIGMA} approach, but do not exceed, the design value of 7×10^{-8}. A similar observation applies to VPL_{H0} risk for this case, i.e., the largest values of CR_{VPLH0} in Figure 6 approach, but do not exceed, the design value of 4×10^{-8}. These results are exactly as expected and serve to confirm the analysis.

Figure 5. DSIGMA Continuity Risk with Both DSIGMA and VPL_{H0} Continuity Constraints

Figure 6. VPL_{H0} Continuity Risk with Both DSIGMA and VPL_{H0} Continuity Constraints

With VPL_{H0} Constraint, Without DSIGMA Constraint

Continuity risk results were computed without the DSIGMA continuity constraint but with the VPL_{H0} constraint. These results were found to be identical to those in Figures 5 and 6. Referring back to Table 1 it can be observed that the theoretical maximum CR_{DSIGMA} with only the VPL_{H0} continuity constraint applied is only slightly larger (1.5×10^{-7}) than the design objective for CR_{DSIGMA} (7×10^{-8}). This prediction and the lack of increase in the maximum CR_{DSIGMA} when the DSIGMA continuity constraint was removed seem to indicate that the VPL_{H0} continuity constraint restricts CR_{DSIGMA} at least as much as does the DSIGMA continuity constraint itself. Consequently, it might conceivably be argued by examination of more locations other than just Seattle that an explicit DSIGMA continuity risk geometry limit is not needed if a VPL_{H0} continuity risk geometry limit is enforced. However, it should be made clear that a similar argument cannot be made with the roles of DSIGMA and VPL_{H0} reversed. That is, implementing a DSIGMA continuity constraint could not alone ensure acceptable VPL_{H0} continuity risk.

AVAILABILITY RESULTS

Of paramount interest in this analysis is the effect of implementing additional continuity constraints for DSIGMA and VPL_{H0} on the availability of adequate satellite geometry. Figure 7 shows a plot of (un)availability results for various cases with and without continuity constraints implemented. The results assume an idealized constellation of 24 satellites in primary orbital slots [11] with constellation state probabilities due to satellite failures corresponding to IFOR objective

9

values [12]. Each bar in a group represents the daily average (un)availability at one of 78 CAT III locations in CONUS.

The first group of results on the left is for the fundamental constraint that VPL_{H0} not exceed a VAL of 10 m. From the graph it can be seen that for this baseline result the typical (un)availability is about 2×10^{-4} with corresponding availability of typically $1 - 2\times10^{-4} = 0.9998$. Note that all other cases add other constraints to this fundamental constraint. The second group of results adds only the VPL_{H0} continuity constraint. The resulting availability decreases to at worst $1 - 4\times10^{-4} = 0.9996$. The third group of results adds only the RRFM continuity constraint. As can be seen from the graph, the addition of RRFM is no more restrictive than is just the fundamental

VPL_{H0} constraint. The fourth group of results adds only the DSIGMA S_{vert} constraints. This case is most restrictive of all with worst availability of about $1 - 6\times10^{-4} = 0.9994$. The fifth group of results adds only the DSIGMA continuity constraint. With availability of no worse than $1 - 3\times10^{-4} = 0.9997$, this case is not as restrictive as is the case adding only the VPL_{H0} continuity constraint. Of course based on the preceding observations it is not surprising that availability for the final set of results implementing all constraints is exactly the same as for adding only the S_{vert} constraints. Consequently, implementing additional constraints for VPL_{H0} and DSIGMA continuity risk would not decrease availability below that achieved when DSIGMA S_{vert} (and RRFM) constraints are implemented as already required.
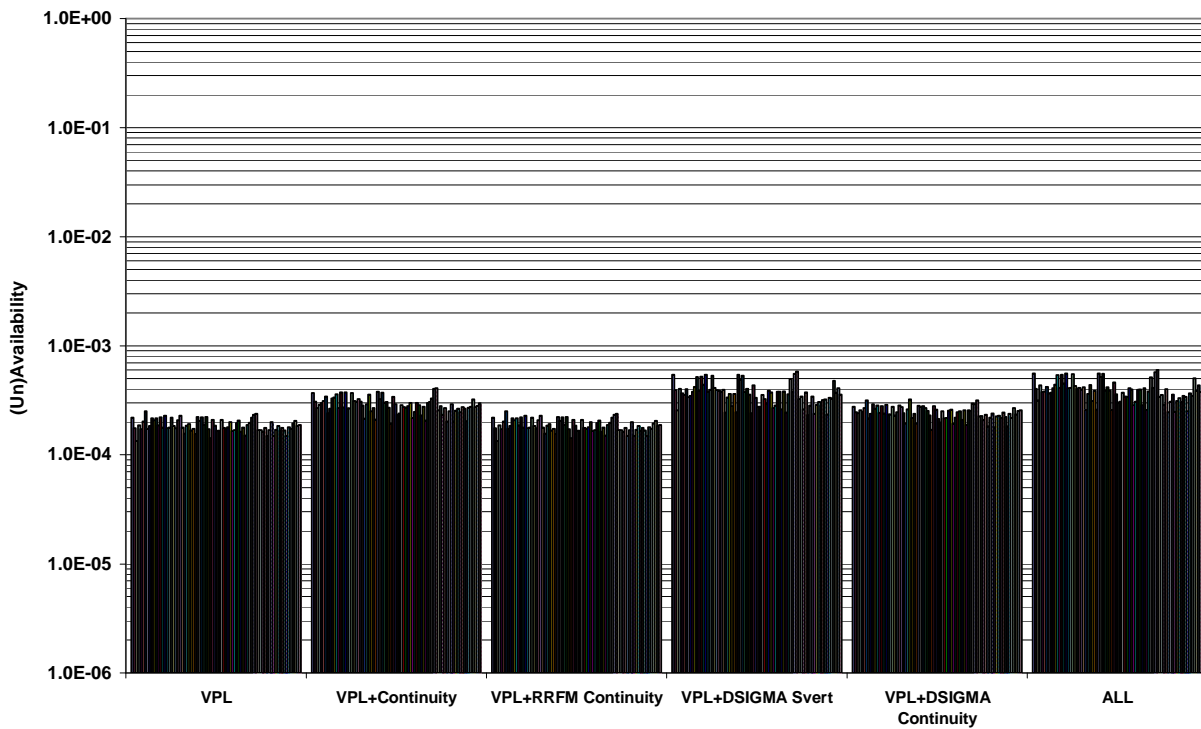

Figure 7. GAST D Availability With and Without Continuity Restrictions

SUMMARY

- Mitigation of ionospheric anomalies involves computing the difference, V_{diff}, between positions based on 30 s smoothed corrections and 100 s smoothed corrections. D_V, the magnitude of V_{diff}, is compared to a threshold by the DSIGMA monitor. Since the 30 s solution is used for navigation, other monitors and protection levels computed in the aircraft must also include the D_V term.

- Since D_V varies in real time, the effect of D_V on continuity risk from monitors and protection levels must be considered.

- Current specifications include a restriction to limit continuity risk from the reference receiver fault monitor (RRFM). These specifications also limit the vertical solution coefficient for any satellite, S_{vert}, in order to ensure adequate integrity from DSIGMA. However, these specifications do not include constraints to limit continuity risk from either

10

DSIGMA or from the VPL_{H0} protection level computation, which will also include D_V.

- The paper has identified continuity constraints needed to separately meet previously proposed continuity risk allocations applied to DSIGMA and VPL_{H0}. These constraints along with the RRFM constraint each independently dictate different limits on the maximum value of σ_{Vdiff}, the standard deviation of V_{diff}. Therefore, theoretical predictions for these limits have been derived in order to study the interplay of the various constraints.

- Illustrative continuity results have been computed for Seattle using an idealized 24 satellite constellation. These results indicate that with just the RRFM constraint, continuity risk values for DSIGMA or for VPL_{H0} are unacceptable. However, with constraints applied, the design values are of course achieved. Furthermore, the VPL_{H0} constraint predominates in such a manner that it alone is arguably sufficient to ensure adequate continuity risk from both VPL_{H0} and DSIGMA.

- Results for availability of adequate satellite geometry indicate that implementing additional constraints for continuity risk from the DSIGMA monitor and VPL_{H0} would not decrease availability below that associated with already specified constraints for RRFM and DSIGMA S_{vert}.

ACKNOWLEDGEMENTS

REFERENCES

1. Burns, J., et al., "Conceptual Framework for the Proposal for GBAS to Support Category III Operations", ICAO NSP/WG-1/WP 11, Montreal CA, 10 – 20 November 2009.

2. FAA, *Specification: Category I Local Area Augmentation System Ground Facility*, FAA-E-2937A, 17 April 2002.

3. RTCA Inc., *Minimum Operational Performance Standards for LAAS Airborne Equipment*, RTCA/DO-253C, 16 December 2008.

4. Murphy, T., & M. Harris, "Mitigation of Ionospheric Gradient Threats for GBAS to Support CAT II/III", *Proceedings of ION GNSS 2006*, Fort Worth, TX, 26 – 29 September 2006.

5. Brenner, Mats & Tim Murphy, private communication, June 2009.

6. Walter, T., et al., "The Effects of Large Ionospheric Gradients on Single Frequency Airborne Smoothing Filters for WAAS and LAAS", *Proceedings of ION National Technical Meeting*, San Diego, CA, 26 – 28 January 2004.

7. McGraw, G., et al., "Development of the LAAS Accuracy Models", *Proceedings of ION GPS 2000*, Salt Lake City, UT, 19 – 22 September 2000.

8. RTCA Inc., *Minimum Aviation System Performance Standards for the Local Area Augmentation System (LAAS)*, RTCA/DO-245, 28 September 1998.

9. M. Harris and Murphy, T., "Geometry Screening for GBAS to Meet CAT III Integrity and Continuity Requirements", *Proceedings of ION National Technical Meeting*, San Diego, CA, 22 – 24 January 2007.

10. Shively, C., "GBAS GAST D Aircraft Monitor Performance Requirements for Single Reference Receiver Faults", *Proceedings of ION International Technical Meeting*, Anaheim, CA, 26 – 28 January 2009.

11. Anon., *Global Positioning System Standard Positioning Service Performance Standard*, Office of Assistant Secretary of Defense for Networks and Information Integration [ASD(NII)/DASD(IC3, Space and Spectrum)], September 2008.

12. FAA, "Interagency Forum on Operational Requirements (IFOR)", 26 July 2004.